Environment. Technology. Resources. Rezekne, Latvia
Proceedings of the 16th International Scientific and Practical Conference.2025. Volume IV, 375-382

Effect of Infill Pattern Design on Tensile Strength of Fused Deposition Modelled Specimens

Jaymin Vrajlal Sanchaniya
Institute of Mechanical and Biomedical Engineering
Riga Technical University
Riga, Latvia
Jaymin.Sanchaniya@rtu.lv

Karunamoorthy Rengasamy Kannathasan
Institute of Mechanical and Biomedical Engineering
Riga Technical University
Riga, Latvia
karunamoorthy.rengasamy-kannathasan@rtu.lv

Sanjay Rajni Vejanand
Institute of Mechanical and Biomedical Engineering
Riga Technical University
Riga, Latvia
sanjay.vejanand@rtu.lv

Jay Joshi
Institute of Mechanical and Biomedical Engineering
Riga Technical University
Riga, Latvia
jay-ashokkumar.joshi@edu.rtu.lv

Inga Lasenko
Institute of Mechanical and Biomedical Engineering
Riga Technical University
Riga, Latvia
inga.lasenko@rtu.lv

***Abstract*—Deep knowledge of the connections between additive manufacturing design elements and the mechanical qualities of additive manufactured products becomes essential as the adoption of technology expands. Research analyses how the arrangement of material inside the printed object affects the tensile strength in specimens made through fused deposition modelling. The evaluation of 18 different infill patterns occurred through standardised tests, while technicians maintained identical processing parameters that included print temperature and both layer height and print speed. The test specimens underwent tensile testing for mechanical analysis. The test results indicate that the concentric pattern delivers maximum elastic modulus values at 1078 MPa, as well as a maximum tensile strength of 26.4 MPa which exceeds other patterns by 12-62% for modulus and 24-98% for strength. The elongation-at-break measurement of 10.5% is the best result for this pattern because it offers 10-338% more flexibility than competing structures. The elastic modulus (665 MPa) and the tensile strength (13.3 MPa) of the lightning pattern are the minimum among all tested patterns. The study also evaluated mass efficiency through strength-to-mass ratio calculations, with the concentric pattern achieving the highest value of 29.7 MPa/g, demonstrating superior weight-normalised mechanical performance alongside its absolute strength advantages. The study provides essential data on the performance-mechanical relationship of infill patterns that allow improvements to additive manufacturing processes to enhance structural integrity. These important results provide guidance for designers working on products that need particular mechanical characteristics.**

Keywords*— *Infill pattern, additive manufacturing, tensile test, fused filament fabrication.

I. Introduction

Additive manufacturing technologies gained speed in development to produce complex structural components with minimal waste while managing small production runs efficiently [1]. The technological progress has triggered worldwide research efforts to use polymers across all dimensional scales from nanoscale to macroscale manufacturing of components [2]–[7]. The adoption of additive manufacturing technologies grows rapidly within different industries where notable advancements occur in automotive [8], aerospace [9], biomedical [10], construction [11], [12] and healthcare applications [13] which extend to dental usage and surgical requirements, orthopaedic implant production, tissue engineering work and pharmaceutical manufacturing [14].

Fused filament fabrication (FFF) represents a cost-friendly and flexible manufacturing method which dominates the production of polymeric, composite, and multimaterial components through 3D printing. FFF technology supports a wide range of thermoplastics beyond acrylonitrile butadiene styrene (ABS), polylactic acid (PLA) [15], polycarbonate (PC) [16] and polyamide (PA) [17] which are the most frequently used plastics. Thermoplastic polyurethane (TPU) [18] along with Polyethylene (PE) [19] and Polypropylene (PP) belong to the elastomer category of materials while polyglycolic acid

Online ISSN 2256-070X
https://doi.org/10.17770/etr2025vol4.8409

(PGA) and polycaprolactone (PCL) fall under the polyesters group, and the advanced engineering polymers group includes polyoxymethylene (POM), polyetheretherketone (PEEK), polyetherimide (PEI), polyphenylene sulphide (PPS), polysulfone (PSU) polyvinylidene fluoride (PVDF) [20].

The weight efficiency of 3D printed components represents another critical aspect of the optimisation of the FFF process that receives insufficient research attention. When mechanical performance is evaluated relative to material usage through metrics such as strength-to-mass ratios, the true practical value of different infill patterns becomes apparent. This consideration becomes particularly relevant in applications where lightweight, yet strong components are required, such as in aerospace and portable biomedical devices. The comparative analysis of weight efficiency metrics complements traditional mechanical testing by revealing which patterns deliver optimal performance per unit mass.

Various design parameters determine the mechanical behaviour of parts created through 3D printing such as extrusion temperature, build plate temperature, printing speed, extrusion speed, print orientation, layer thickness, raster angle, width and air gaps, nozzle diameter, ambient temperature and humidity, and infill pattern with density [21]–[25]. The influence of infill patterns on mechanical strength receives less research attention than other FFF process parameters, including layer thickness and raster width and orientation.

The analysis of infill patterns in previous research focused on limited options, but the available patterns continue to grow to cover various applications [26]–[29]. Analysis of infill patterns consists of rectilinear, honeycomb, Hilbert curve, octagram, star-shaped, and triangular arrangements. Standardised research does not exist to evaluate the 18 different fill patterns that exist today. This research fills the current knowledge gap by performing a systematic pattern-by-pattern comparison of all 18 infill designs using PLA material, which reveals crucial findings about FFF-manufactured component performance and pattern selection.

II. Materials and Methodology

The test samples used commercial filaments (Prusa Research a.s., Czech Republic) that had 1.75 mm diameter. The specimens followed the dimensioning requirements of ISO 527-5A and received printing on a Prusa Mini machine that used a glass fibre build plate.

The production of complete test specimens using PLA relied on the conditions and parameters presented in Table 1 for the consistency of the FFF process. The drying process at 40 °C for one hour (using eSUN eBOX Lite) was designed to remove moisture and prevent potential manufacturing problems in both the print quality and the mechanical characteristics of the material.

Table 1 Summary of FFF Process Conditions and Parameters

Printing specifications	Value, description
Filament (Ø 1.75 mm)	PLA
3D printer	Prusa Mini
Printer chamber	Semi-open
Nozzle diameter (mm)	0.4
Build plate	Glass fibre
Extrusion temperature (°C)	230
Built plate temperature (°C)	65
Print speed (mm/s)	25
Layer thickness (mm)	0.1
Shell thickness (mm)	0.1 mm
Infill density (%)	40

A layer thickness of 0.1 mm was selected as an optimal compromise between structural integrity [20], mechanical performance, and production efficiency. The width of the infill line (raster) was automatically configured by PrusaSlicer to approximately 0.35 mm when using a 0.4 mm diameter nozzle. All printed samples featured patterned infills encapsulated within a 0.1 mm thickness.

While maintaining all other parameters constant, 18 distinct infill patterns with the mentioned designation: Rectilinear (S1), Aligned Rectilinear (S2), Grid (S3), Triangles (S4), Stars (S5), Cubic (S6), Line (S7), Concentric (S8), Honeycomb (S9), 3D Honeycomb (S10), Gyroid (S11), Hilbert curve (S12), Archimedean Chords (S13), Octagram Spiral (S14), Adaptive Cubic (S15), Support Cubic (S16), Lightning (S17) and Zig Zag (S18). Figure 1 illustrates all of the 18 fill patterns used in this study.

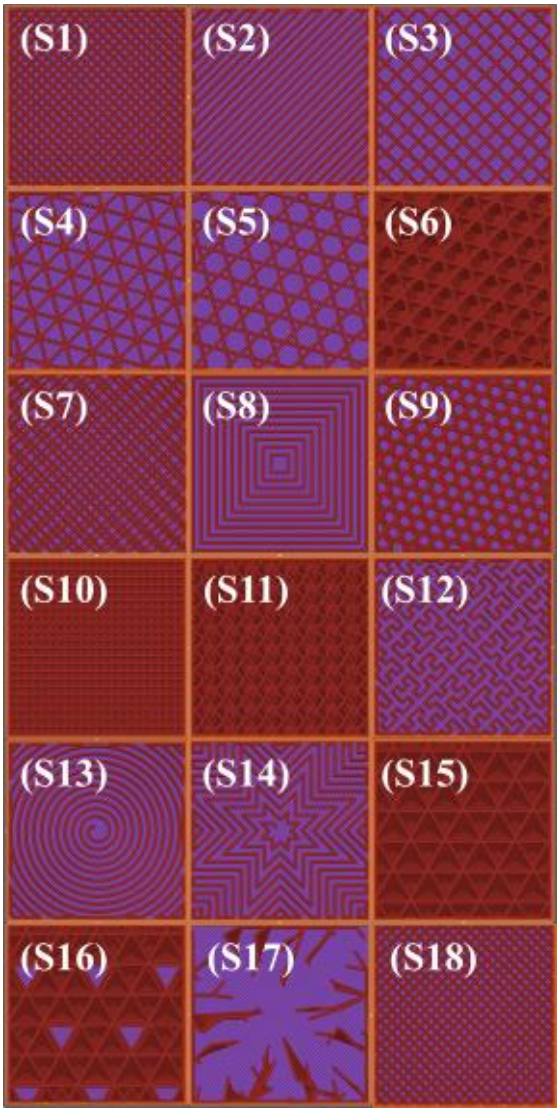

Fig. 1. Visualization of the eighteen infill patterns tested in this study: Rectilinear (S1), Aligned Rectilinear (S2), Grid (S3), Triangles (S4), Stars (S5), Cubic (S6), Line (S7), Concentric (S8), Honeycomb (S9), 3D Honeycomb (S10), Gyroid (S11), Hilbert curve (S12), Archimedean Chords (S13), Octagram Spiral (S14), Adaptive Cubic (S15), Support Cubic (S16), Lightning (S17) and Zig Zag (S18).

Tensile testing of 90 specimens used five replicate samples for each infill pattern design. The experimental tests were executed on a Mecmesin Multi-Test 2.5-i tensile testing machine from PPT Group UK Ltd. (traded as Mecmesin, based in Slinfold, UK) provided with a 250 N sensor. All test conditions received a 1 mm/min uniaxial tensile loading rate as a standardised delivery speed.

Figure 2 illustrates one group of prepared specimens manufactured according to the specified standards.

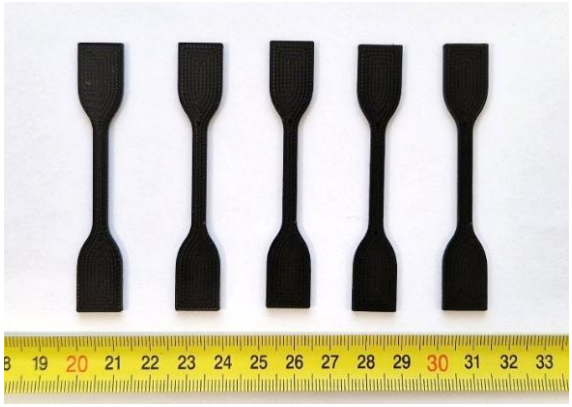

Fig. 2. ISO 527-5A compliant tensile test specimens produced by FFF.

Standardised testing procedures allowed researchers to obtain accurate measurements of mechanical properties, which included elastic modulus along with the ultimate tensile strength and elongation at break. The method provided standardised procedures for valid comparison testing of different fill structures by controlling experimental factors, which are shown in Table 1. Before testing, the specimens were kept under controlled ambient conditions to avoid environmental factors (temperature 23 °C ± 1, relative humidity 30-50%, standard atmospheric pressure: 1 atm) that could alter the results. Mass measurements were performed using a high-precision KERN ABT 5NM scale, which boasts a maximum capacity of 100 g and a precision of 0.000001 g, thus ensuring accurate and reliable results.

III. Results and Discussion

A. Tensile Behaviour of Different Infill Patterns

Tests of 18 different infilled sample arrangements showed substantial variations in their mechanical properties through tensile experiments. Representative stress-strain curves exist for each designation of the infill pattern (S1-S18) which demonstrates different uniaxial loading behaviours as shown in Figure 3.

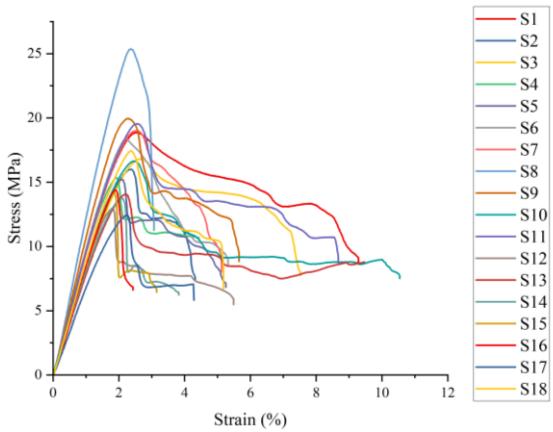

Fig. 3. Representative stress-strain curves for 18-different infill patterns (S1-S18).

The stress-strain curves show elastic behaviour as their first stage and then exhibit yielding before entering the plastic deformation portion. There is a substantial range of elastic modulus combined with maximum tensile strength and elongation at break differences between the tested infill patterns. Patterns S1, S8, and S11 displayed stress peaks that resulted in stepwise failures, while patterns S10 and S13 showed sustained stretching abilities before failure occurred.

S8 showed the strongest mechanical results through its 1078 ± 45 MPa elastic modulus and 26.4 ± 2.3 MPa ultimate tensile strength. Pattern architecture advances stress distribution because its circular loop design spreads tensile loads evenly throughout the entire structure. The tensile loading direction of the material in the deposit promotes beneficial strain patterns throughout the sample area.

The total results of the tensile test demonstrated the lightning pattern (S17) was the weakest arrangement since it contained the lowest elastic modulus (665 ± 61 MPa) coupled with the weakest tensile strength (13.3 ± 1.9 MPa). The lightning pattern displays critical weaknesses that lead to a substantial reduction in elastic modulus (38% less than the concentric pattern) and ultimate tensile strength (50% weaker than the concentric pattern). Material reduction takes priority at the expense of structural integrity in this design. Experiment results shows that the randomly created non-uniform path format within the print structure introduces serious weaknesses, which deteriorate when exposed to tensile forces.

Mass measurements revealed significant variations between the different infill pattern configurations. The lightest specimen was the lightning pattern (S17) at 0.661 g, while the honeycomb pattern (S9) produced the heaviest specimens at 0.974 g, representing a 47% difference in material usage. This weight variation directly impacts the practical application of these patterns, particularly in weight-sensitive contexts.

Regarded as one of the best performers, the 3D honeycomb pattern (S10) achieved an outstanding elongation at a break value of 10.5 ± 1.4% which exceeded all other pattern configurations with respect to flexibility and failure deformation capacity. Multiple layers of interconnected cells in the structure enable progressive deformation, for which ductility improves significantly.

All tested infill patterns received a full analysis of mechanical properties in Table 2 using elastic modulus, ultimate tensile strength, and elongation at break measurements.

The elastic modulus measurements spanned from 665 ± 61 MPa, to 1078 ± 45 MPa while showing a total difference of 62% between the tested patterns. The maximum tensile strength measured between 13.3 ± 1.9 MPa and 26.4 ± 2.3 MPa and created a 98% difference between the lowest and highest values. The ductility performance demonstrated the largest variation because the elongation at break results reached between 2.4% and 10.5%, resulting in a 338% difference between the patterns.

TABLE 2 SUMMARRY OF MECHANICAL PROPERTIES AND WEIGHT FOR 18 INFILL PATTERNS

No.	Pattern Type	Elastic Modulus, E MPa	Ultimate Tensile Strength, σ_{max} MPa	Elongation at Break, Strain ε %	Mass (g)	S:M ratio (MPa/g)
S1	Recti-linear	930 ± 84	20.1 ± 1.1	9.3 ± 1.8	0.893	22.5
S2	Aligned Recti-linear	795 ± 80	17.2 ± 2.3	4.3 ± 0.6	0.884	19.4
S3	Grid	850 ± 52	17.7 ± 1.2	7.5 ± 0.8	0.842	21.0
S4	Triangles	912 ± 82	16.8 ± 0.9	4.5 ± 0.3	0.871	19.2
S5	Stars	837 ± 46	16.2 ± 1.5	5.2 ± 0.9	0.847	19.1
S6	Cubic	942 ± 85	19.2 ± 1.7	5.3 ± 0.7	0.865	22.2
S7	Line	948 ± 76	20.1 ± 1.9	5.1 ± 0.4	0.884	22.74
S8	Concen-tric	1078 ± 45	26.4 ± 2.3	3.0 ± 0.3	0.889	29.7
S9	Honeycomb	971 ± 67	21.1 ± 3.1	5.6 ± 0.9	0.974	21.6
S10	3D honey-comb	892 ± 98	17.7 ± 2.3	10.5 ± 1.4	0.887	19.9
S11	Gyroid	915 ± 57	20.4 ± 1.2	8.7 ± 0.9	0.854	23.8
S12	Hilbert Curve	851 ± 65	14.0 ± 1.1	5.5 ± 0.6	0.898	15.5
S13	Archimedean Chords	730 ± 92	15.3 ± 2.7	9.5 ± 1.6	0.879	17.4
S14	Octagram Spiral	785 ± 81	14.9 ± 1.1	3.8 ± 0.6	0.885	16.8
S15	Adaptive Cubic	820 ± 73	15.2 ± 1.7	3.1 ± 0.2	0.757	20.1
S16	Support Cubic	790 ± 55	15.3 ± 1.5	2.4 ± 0.2	0.760	20.1
S17	Lightning	665 ± 61	13.3 ± 1.9	4.3 ± 0.5	0.661	20.1
S18	Zig Zag	837 ± 74	18.5 ± 1.1	5.1 ± 1	0.869	21.3

The rectilinear pattern (S1) maintained balanced mechanical properties that featured moderate strength of 20.1 ± 1.1 MPa alongside good elongation capacity of 9.3 ± 1.8%. The orthogonal design of this pattern combines strong tensile resistance with sufficient ductility properties. The gyroid pattern (S11) exhibited balanced performance characteristics because it showed a strength of 20.4 ± 1.2 MPa in addition to an elongation of 8.7 ± 0.9% elongation.

The representative sample in Figure 4 shows failure that occurred within the gauge length thus validating the testing methodology.

Fig. 4. Representative fractured tensile sample showing stress concentration in the centre region.

Each fracture surface showed distinct characteristics related to the patterns used in the infill. Massive plastic deformation occurred before failure on fracture surfaces which appeared irregular due to flexible patterns (3D honeycomb, Archimedean chords) while specimens with rigid patterns (concentric, rectilinear) presented neat fracture surfaces with minor necking.

B. Pattern-Specific Performance Analysis

The mechanical response depends heavily on the way the materials get arranged during the printing process. Patterns featuring continuous filament alignment parallel to the tensile force direction (concentric-S8 and rectilinear aligned-S2) produced better tensile strength than patterns having mainly perpendicular or angular material distributions [30], [31].

A continuous circular path in the concentric pattern (S8) provides outstanding performance by aligning materials with tensile loading and minimising interlayer bond weakness which results in tensile strength of 26.4 ± 2.3 MPa [32]. The structural alignment system distributes stresses across all components until failure occurs at all points simultaneously [33].

The 3D honeycomb structure (S10) achieves its high elongation of 10.5% because its three-dimensional configuration allows the material to stretch progressively between multiple layers [34]. The geometric arrangement allows the pattern to function by deforming locally until it reaches failure but avoids complete failure and enables substantial plastic deformation before total separation [35].

The lightning pattern (S17) and support cubic (S16) showcase the worst mechanical performance because their nonuniform material distribution patterns lead to a low strength value of 13.3 ± 1.9 MPa and minimal elongation capability of 2.4% [36]. The structural weaknesses within these patterns stem from their design choice of material reduction and functional needs, which overrides mechanical performance [37].

The grid pattern (S3) achieved moderate success in all mechanical testing results (850 ± 52 MPa modulus, 17.7 ± 2.3 MPa strength, 7.5% elongation) because it optimises mechanical behaviour without surpassing any particular requirement.

When analysing mechanical performance relative to material usage, the concentric pattern (S8) demonstrated exceptional efficiency with a strength-to-mass ratio of 29.7 MPa/g. This represents a 92% improvement over the least efficient pattern, the Hilbert curve (S12), which achieved only 15.5 MPa/g. The gyroid pattern (S11) also performed admirably in weight-normalised terms with an S:M ratio of 23.8 MPa/g, highlighting its potential for applications where both strength and weight considerations are critical.

C. Relationship Between Pattern Design and Mechanical Properties

The results show multiple key connections that exist between the designed infill pattern features and the mechanical outcomes.

- The mechanical strength of specimen produced via FFF increased when parallel material paths were used as concentric (S8) or rectilinear patterns (S1) [38], [39].
- Ductility and elongation improved when using three-dimensional interconnected structures which include the 3D honeycomb (S10) and gyroid patterns (S11) [40].
- The perpendicular material orientation in the cubic (S6) and lightning patterns (S17) reduced mechanical strength and stiffness to a significant extent [41].
- Mechanical performance improved independently of geometric complexity because the simple concentric pattern exceeded both the Hilbert curve (S12) and octagram spiral designs (S14) [42].
- The weight efficiency varied substantially between the patterns, with the concentric pattern (S8) achieving the highest strength-to-mass ratio of 29.7 MPa/g, while patterns with complex geometries such as the Hilbert curve (S12) showed lower efficiency at 15.5 MPa/g despite using similar amounts of material.

The mechanical properties of 3D printed objects depend mainly on three factors, including material orientation compared to structural stress [43], the uninterrupted nature of the printing path [44] as well as the complete network of printed material throughout the component [45]. The mechanical properties of the optimised factors improved in every design independently of the dimensional complexity [46].

The study presents thorough performance assessments of infill patterns, but readers should note its underlying restrictions. The study results only apply to the design of the standardised test specimen design used for this research. The relative performance between patterns can change with different component aspects along with dimension variations due to scaling effects and geometry-based stress distributions.

The mechanical properties remain valid only for PLA material processed under the described conditions. Materials with distinctive crystallinity levels and different molecular weights and additive components may show different relative performances of the infill patterns. Different infill patterns may show changes in their relative performance levels due to environmental factors which include ambient temperature, humidity, and ageing effects.

Standard tensile testing occurs at 1 mm/min strain rate and ambient temperature to generate comparable results yet fails to replicate dynamic loading conditions or high temperatures and creep effects. Future studies which will examine performance under different loading conditions.

Despite certain limitations, the extensive study of 18 unique infill patterns gives engineers valuable tools to select appropriate patterns that maximise component performance according to specific use requirements.

IV. CONCLUSION

The extensive research analysed 18 infill patterns which produced substantial differences in the mechanical characteristics of FDM-printed PLA specimens. The concentric pattern (S8) exhibited superior structural properties because it achieved the highest elastic modulus at 1078 ± 45 MPa along with the ultimate tensile strength at 26.4 ± 2.3 MPa, yet the 3D honeycomb pattern showed remarkable elongation capabilities at 10.5%. The research findings demonstrate that pattern shapes affect mechanical characteristics through path alignment internation and interconnecting forms that enhance performance.

Beyond absolute mechanical performance, the study also revealed significant variations in mass efficiency in all the tested patterns. The concentric pattern not only exhibited superior mechanical properties, but also demonstrated the highest strength-to-mass ratio at 29.7 MPa/g, which represents a critical metric for weight-sensitive applications. This efficiency parameter provides designers with an additional selection criterion when optimising components for specific use cases where both strength and weight considerations are paramount. Substantial variations in S:M ratios—ranging from 15.5 to 29.7 MPa / g, highlight the importance of pattern selection for weight-efficient design in additive manufacturing.

Pattern selection emerges as a vital design parameter for additive manufacturing because it leads to significant variations in performance levels that reach up to 62% in modulus and 98% in strength and 338% in elongation. Research provides quantitative engineering recommendations which allow designers to enhance component performance by matching infill patterns to application needs, thus improving procedures and structural robustness in 3D-printed parts.

V. ACKNOWLEDGEMENTS

This work has been supported by postdoctoral grant No RTU-ZG-2024/1-0048 under the EU Recovery and Resilience Facility funded project No. 5.2.1.1.i.0/2/24/I/CFLA/003 “Implementation of consolidation and management changes at Riga Technical University, Liepaja University, Rezekne Academy of Technology, Latvian Maritime Academy and Liepaja Maritime College for the progress towards excellence in higher education, science, and innovation”.

REFERENCES

[1] S. Salifu, D. Desai, O. Ogunbiyi, and K. Mwale, “Recent development in the additive manufacturing of polymer-based composites for automotive structures—a review,” *Int. J. Adv. Manuf. Technol.*, vol. 119, no. 11, pp. 6877–6891, 2022, doi: 10.1007/s00170-021-08569-z.

[2] J. V. Sanchaniya *et al.*, “A Novel Method to Enhance the Mechanical Properties of Polyacrylonitrile Nanofiber Mats: An Experimental and Numerical Investigation,” *Polymers (Basel).*, vol. 16, no. 7, p. 992, Apr. 2024, doi: 10.3390/polym16070992.

[3] J. V. Sanchaniya, I. Lasenko, V. Gobins, and A. Kobeissi, “A Finite Element Method for Determining the Mechanical Properties of Electrospun Nanofibrous Mats,” *Polym.*, vol. 16, no. 6, p. 852, 2024, doi: 10.3390/polym16060852.

[4] J. V. Sanchaniya *et al.*, “Mechanical and Thermal Characterization of Annealed Oriented PAN Nanofibers,” *Polymers (Basel).*, vol. 15, no. 15, 2023, doi: 10.3390/polym15153287.

[5] J. V. Sanchaniya, I. Lasenko, S. P. Kanukuntla, A. Mannodi, A. Viluma-gudmona, and V. Gobins, “Preparation and Characterization of Non-Crimping Laminated Textile Composites Reinforced with Electrospun Nanofibers,” *Nanomaterials*, vol. 13, no. 13, p. 1949, 2023, doi: 10.3390/nano13131949.

[6] K. R. Kannasthan, A. Krasnikovs, and A. Macanovskis, “Ingredients Degradation in Steel Fiber Reinforced Concrete after Thermal Loading,” *Vide. Tehnol. Resur. - Environ. Technol. Resour.*, vol. 3, pp. 124–128, 2023, doi: 10.17770/etr2023vol3.7228.

[7] O. Kononova, V. Lusis, A. Galushchak, A. Krasnikovs, and A. Macanovskis, “Numerical modeling of fiber pull-out micromechanics in concrete matrix composites,” *J. Vibroengineering*, vol. 14, no. 4, pp. 1852–1861, 2012.

[8] J. C. Vasco, “Chapter 16 - Additive manufacturing for the automotive industry,” in *Handbooks in Advanced Manufacturing*, J. Pou, A. Riveiro, and J. P. B. T.-A. M. Davim, Eds. Elsevier, 2021, pp. 505–530. doi: https://doi.org/10.1016/B978-0-12-818411-0.00010-0.

[9] B. Blakey-Milner *et al.*, “Metal additive manufacturing in aerospace: A review,” *Mater. Des.*, vol. 209, p. 110008, 2021, doi: https://doi.org/10.1016/j.matdes.2021.110008.

[10] R. Kumar, M. Kumar, and J. S. Chohan, “The role of additive manufacturing for biomedical applications: A critical review,” *J. Manuf. Process.*, vol. 64, pp. 828–850, 2021, doi: https://doi.org/10.1016/j.jmapro.2021.02.022.

[11] A. Macanovskis, A. Krasnikovs, O. Kononova, and A. Lukasenoks, “Mechanical Behavior of Polymeric Synthetic Fiber in the Concrete,” *Procedia Eng.*, vol. 172, pp. 673–680, 2017, doi: 10.1016/j.proeng.2017.02.079.

[12] V. Lusis, K. K. Annamaneni, and A. Krasnikovs, "Concrete Reinforced by Hybrid Mix of Short Fibers under Bending," *Fibers*, vol. 10, no. 2, p. 11, Jan. 2022, doi: 10.3390/fib10020011.

[13] E. Rezvani Ghomi, F. Khosravi, R. E. Neisiany, S. Singh, and S. Ramakrishna, "Future of additive manufacturing in healthcare," *Curr. Opin. Biomed. Eng.*, vol. 17, p. 100255, 2021, doi: https://doi.org/10.1016/j.cobme.2020.100255.

[14] C. I. Gioumouxouzis, C. Karavasili, and D. G. Fatouros, "Recent advances in pharmaceutical dosage forms and devices using additive manufacturing technologies," *Drug Discov. Today*, vol. 24, no. 2, pp. 636–643, 2019, doi: https://doi.org/10.1016/j.drudis.2018.11.019.

[15] R. S. Odera and C. I. Idumah, "Novel advancements in additive manufacturing of PLA: A review," *Polym. Eng. Sci.*, vol. 63, no. 10, pp. 3189–3208, 2023, doi: 10.1002/pen.26450.

[16] K. Bulanda *et al.*, "Polymer Composites Based on Polycarbonate (PC) Applied to Additive Manufacturing Using Melted and Extruded Manufacturing (MEM) Technology," *Polymers*, vol. 13, no. 15. 2021. doi: 10.3390/polym13152455.

[17] J. M. Jafferson and D. Chatterjee, "A review on polymeric materials in additive manufacturing," *Mater. Today Proc.*, vol. 46, pp. 1349–1365, 2021, doi: https://doi.org/10.1016/j.matpr.2021.02.485.

[18] S. M. Desai, R. Y. Sonawane, and A. P. More, "Thermoplastic polyurethane for three-dimensional printing applications: A review," *Polym. Adv. Technol.*, vol. 34, no. 7, pp. 2061–2082, 2023, doi: 10.1002/pat.6041.

[19] F. Christakopoulos, P. M. H. van Heugten, and T. A. Tervoort, "Additive Manufacturing of Polyolefins," *Polymers*, vol. 14, no. 23. 2022. doi: 10.3390/polym14235147.

[20] F. N. Mullaveettil, R. Dauksevicius, and Y. Wakjira, "Strength and elastic properties of 3D printed PVDF-based parts for lightweight biomedical applications," *J. Mech. Behav. Biomed. Mater.*, vol. 120, no. March, p. 104603, 2021, doi: 10.1016/j.jmbbm.2021.104603.

[21] M. Golab, S. Massey, and J. Moultrie, "How generalisable are material extrusion additive manufacturing parameter optimisation studies? A systematic review," *Heliyon*, vol. 8, no. 11, p. e11592, 2022, doi: 10.1016/j.heliyon.2022.e11592.

[22] J. Beniak, M. Holdy, P. Križan, and M. Matúš, "Research on parameters optimization for the Additive Manufacturing process," *Transp. Res. Procedia*, vol. 40, pp. 144–149, 2019, doi: https://doi.org/10.1016/j.trpro.2019.07.024.

[23] K. Walia, A. Khan, and P. Breedon, "Polymer-Based Additive Manufacturing: Process Optimisation for Low-Cost Industrial Robotics Manufacture," *Polymers*, vol. 13, no. 16. 2021. doi: 10.3390/polym13162809.

[24] I. Baturynska, O. Semeniuta, and K. Martinsen, "Optimization of Process Parameters for Powder Bed Fusion Additive Manufacturing by Combination of Machine Learning and Finite Element Method: A Conceptual Framework," *Procedia CIRP*, vol. 67, pp. 227–232, 2018, doi: https://doi.org/10.1016/j.procir.2017.12.204.

[25] N. Mohan, P. Senthil, S. Vinodh, and N. Jayanth, "A review on composite materials and process parameters optimisation for the fused deposition modelling process," *Virtual Phys. Prototyp.*, vol. 12, no. 1, pp. 47–59, Jan. 2017, doi: 10.1080/17452759.2016.1274490.

[26] S. F. Khan, H. Zakaria, Y. L. Chong, M. A. M. Saad, and K. Basaruddin, "Effect of infill on tensile and flexural strength of 3D printed PLA parts," *IOP Conf. Ser. Mater. Sci. Eng.*, vol. 429, no. 1, 2018, doi: 10.1088/1757-899X/429/1/012101.

[27] P. K. Mishra, P. Senthil, S. Adarsh, and M. S. Anoop, "An investigation to study the combined effect of different infill pattern and infill density on the impact strength of 3D printed polylactic acid parts," *Compos. Commun.*, vol. 24, p. 100605, 2021, doi: https://doi.org/10.1016/j.coco.2020.100605.

[28] N. S. Hmeidat, B. Brown, X. Jia, N. Vermaak, and B. Compton, "Effects of infill patterns on the strength and stiffness of 3D printed topologically optimized geometries," *Rapid Prototyp. J.*, vol. 27, no. 8, pp. 1467–1479, Jan. 2021, doi: 10.1108/RPJ-11-2019-0290.

[29] M. Lalegani Dezaki, M. K. Ariffin, A. Serjouei, A. Zolfagharian, S. Hatami, and M. Bodaghi, "Influence of Infill Patterns Generated by CAD and FDM 3D Printer on Surface Roughness and Tensile Strength Properties," *Applied Sciences*, vol. 11, no. 16. 2021. doi: 10.3390/app11167272.

[30] F. A. Kucherov, E. G. Gordeev, A. S. Kashin, and V. P. Ananikov, "Three-Dimensional Printing with Biomass-Derived PEF for Carbon-Neutral Manufacturing," *Angew. Chemie - Int. Ed.*, vol. 56, no. 50, pp. 15931–15935, 2017, doi: 10.1002/anie.201708528.

[31] J. M. Chacón, M. A. Caminero, E. García-Plaza, and P. J. Núñez, "Additive manufacturing of PLA structures using fused deposition modelling: Effect of process parameters on mechanical properties and their optimal selection," *Mater. Des.*, vol. 124, pp. 143–157, 2017, doi: https://doi.org/10.1016/j.matdes.2017.03.065.

[32] V. Mazzanti, L. Malagutti, and F. Mollica, "FDM 3D Printing of Polymers Containing Natural Fillers: A Review of their Mechanical Properties," *Polymers*, vol. 11, no. 7. 2019. doi: 10.3390/polym11071094.

[33] G. Dong, G. Wijaya, Y. Tang, and Y. F. Zhao, "Optimizing process parameters of fused deposition modeling by Taguchi method for the fabrication of lattice structures," *Addit. Manuf.*, vol. 19, pp. 62–72, 2018, doi: https://doi.org/10.1016/j.addma.2017.11.004.

[34] J.-Y. Lee, J. An, and C. K. Chua, "Fundamentals and applications of 3D printing for novel materials," *Appl. Mater. Today*, vol. 7, pp. 120–133, 2017, doi: https://doi.org/10.1016/j.apmt.2017.02.004.

[35] G. D. Goh, Y. L. Yap, S. Agarwala, and W. Y. Yeong, "Recent Progress in Additive Manufacturing of Fiber Reinforced Polymer Composite," *Adv. Mater. Technol.*, vol. 4, no. 1, pp. 1–22, 2019, doi: 10.1002/admt.201800271.

[36] A. Cattenone, S. Morganti, G. Alaimo, and F. Auricchio, "Finite Element Analysis of Additive Manufacturing Based on Fused Deposition Modeling: Distortions Prediction and Comparison With Experimental Data," *J. Manuf. Sci. Eng.*, vol. 141, no. 1, Nov. 2018, doi: 10.1115/1.4041626.

[37] T. J. Hoskins, K. D. Dearn, and S. N. Kukureka, "Mechanical performance of PEEK produced by additive manufacturing," *Polym. Test.*, vol. 70, pp. 511–519, 2018, doi: https://doi.org/10.1016/j.polymertesting.2018.08.008.

[38] A. Rodríguez-Panes, J. Claver, and A. M. Camacho, "The Influence of Manufacturing Parameters on the Mechanical Behaviour of PLA and ABS Pieces Manufactured by FDM: A Comparative Analysis," *Materials*, vol. 11, no. 8. 2018. doi: 10.3390/ma11081333.

[39] M. Moradi, A. Aminzadeh, D. Rahmatabadi, and A. Hakimi, "Experimental investigation on mechanical characterization of 3D printed PLA produced by fused deposition modeling (FDM)," *Mater. Res. Express*, vol. 8, no. 3, 2021, doi: 10.1088/2053-1591/abe8f3.

[40] L. Yang, O. Harrysson, H. West, and D. Cormier, "Mechanical properties of 3D re-entrant honeycomb auxetic structures realized via additive manufacturing," *Int. J. Solids Struct.*, vol. 69–70, pp. 475–490, 2015, doi: https://doi.org/10.1016/j.ijsolstr.2015.05.005.

[41] M. Domingo-Espin, J. M. Puigoriol-Forcada, A.-A. Garcia-Granada, J. Llumà, S. Borros, and G. Reyes, "Mechanical property characterization and simulation of fused deposition modeling Polycarbonate parts," *Mater. Des.*, vol. 83, pp. 670–677, 2015, doi: https://doi.org/10.1016/j.matdes.2015.06.074.

[42] L. M. Galantucci, I. Bodi, J. Kacani, and F. Lavecchia, "Analysis of Dimensional Performance for a 3D Open-source Printer Based on Fused Deposition Modeling Technique," *Procedia CIRP*, vol. 28, pp. 82–87, 2015, doi: https://doi.org/10.1016/j.procir.2015.04.014.

[43] T. Yao, Z. Deng, K. Zhang, and S. Li, "A method to predict the ultimate tensile strength of 3D printing polylactic acid (PLA) materials with different printing orientations," *Compos. Part B Eng.*, vol. 163, pp. 393–402, 2019, doi: https://doi.org/10.1016/j.compositesb.2019.01.025.

[44] R. J. Zaldivar, D. B. Witkin, T. McLouth, D. N. Patel, K. Schmitt, and J. P. Nokes, "Influence of processing and orientation print effects on the mechanical and thermal behavior of 3D-Printed ULTEM® 9085 Material," *Addit. Manuf.*, vol. 13, pp. 71–80, 2017, doi:

https://doi.org/10.1016/j.addma.2016.11.007.

[45] M. K. Thompson *et al.*, "Design for Additive Manufacturing: Trends, opportunities, considerations, and constraints," *CIRP Ann.*, vol. 65, no. 2, pp. 737–760, 2016, doi: https://doi.org/10.1016/j.cirp.2016.05.004.

[46] I. Chiulan, A. N. Frone, C. Brandabur, and D. M. Panaitescu, "Recent Advances in 3D Printing of Aliphatic Polyesters," *Bioengineering*, vol. 5, no. 1. 2018. doi: 10.3390/bioengineering5010002.